FLEXURAL RIGIDITY FOR ANALYSIS OF CONCRETE ARCH BRIDGES

MAREK K. KOŁODZIEJCZYK, *e-mail: mkk0010@auburn.edu*
J. MICHAEL STALLINGS
Department of Civil Engineering, Auburn University, Auburn, AL, USA

TRAVIS H. LE
Structural Associate
Nuclear Power Technologies
Sargent & Lundy, L. L. C., Chattanooga, TN, USA

Abstract: A load rating was performed for a reinforced concrete arch bridge that was opened for traffic in 1931. Use of elastic second-order analysis resulted in a calculated capacity approximately 20% higher than that found using the AASHTO moment magnifier method. Elastic second-order analysis requires modeling of the flexural rigidity, EI, of the arch cross section. Commonly used methods for modeling EI are described, and second-order analysis results are presented to illustrate the sensitivity of the results to the modeling approach. For the arch considered here, the moment magnification was insignificant when the effective EI value was approximately 40% or more of the value obtained by multiplying the short-term modulus of elasticity by the gross moment of inertia of the cross section. Results illustrated that the moment magnification can be significant for concrete with a large ultimate creep coefficient.

Keywords: flexural rigidity, arch bridge, reinforced concrete, structural evaluation, slenderness, second-order analysis

1. Introduction

A load rating of the Bibb Graves Bridge was performed for the Alabama Department of Transportation (ALDOT) using the Load Factor Rating (LFR) method defined in *The Manual for Bridge Evaluation* (1). The Bibb Graves Bridge shown in Figure 1 is a seven-span reinforced concrete arch bridge that spans the Coosa River in Wetumpka, Alabama. The bridge was opened for traffic in 1931. One of the bridge spans is experiencing deterioration due to Alkali-Silica reactivity. The work reported here is from an initial evaluation of the bridge without regard for the deterioration. Preliminary ratings of the arch rib of one of the spans (Span V) indicated a capacity of only 81% of an ALDOT standard 37.5-ton tri-axle dump truck. This rating was significantly lower than the ratings determined for the transverse floor-beams which were eventually found to control the load rating. The low rating for the arch rib was attributed primarily to the use of the moment magnifier method that is a part of AASHTO's *Standard Specifications for Highway Bridges* (2) for in-plane slenderness effects for arches. Second-order analyses of the arch rib resulted in significantly higher capacity. Reported here is a description of common methods that are available for modeling the flexural rigidity, EI, of an arch rib in elastic second-order analysis. Analysis results are provided for one span of the Bibb-Graves Bridge (Span V) to illustrate the impact of the flexural rigidity on the slenderness effect. A complete report of the investigation of slenderness effects and the bridge rating analyses is provided by Le and Stallings (3).

Spans III through VII of the Bibb Graves Bridge are shown from left to right in Figure 1. The five spans at the center of the bridge are symmetric half-through type parabolic arches (4) and the roadway is supported at approximately mid-height of the arches. The spans at each end are non-symmetric deck type arches with the arches completely below the roadway. The roadway deck varies from 7 in. to 8 in. in thickness and is supported by transverse floorbeams at spacings between 8.75 ft and 11.0 ft in the various arch spans. Spandrel columns support transverse floorbeams where the roadway is above the arch, and reinforced concrete tension hangers support the floorbeams where the roadway is below the arch. The bridge is essentially symmetric about the center span, Span IV. Span V is used for the comparisons presented here. The arch ribs of Span V have a span length of 128 ft, rise of 44.6 ft, rib thickness at the crown of 27.0 in., and rib thickness at the base of 46.6 in. The width of the arch rib cross section is constant at 48 in.

2. Bridge description and basic model

Fig. 1. Bibb Graves Bridge in Wetumpka, Alabama

The reinforcement at the top and bottom of each arch varied from 0.4 to 0.7 percent of the gross concrete area. A structural analysis model of a typical arch rib is shown in Figure 2. Each arch is modeled with a two-dimensional model. The roadway consists of a deck slab on transverse floorbeams, the roadway is modeled as a system of simple spans supported by the columns and hangers that are pin-ended links. These modeling assumptions are consistent with the assumptions made in the analysis and rating of the transverse floorbeams, tension hangers and columns. Specifically, truck loads are distributed to the transverse floorbeams assuming the deck to act as simple beams (AASHTO (2) Table 3.23.3.1, footnote f), and the concrete hangers are assumed to be cracked so that the flexural stiffness of the hangers is negligible. As a result of the modeling assumptions, the roadway, columns, and hangers comprise a statically determinate system that transfers the truck loading to the arch. Also as a result, the deck hangers and columns do not provide bracing or rotational restraint for the arch, so the results presented here are for a worst case that will produce the largest slenderness effects. There is a transverse finger joint in the deck at midspan, so the roadway on each side of midspan is cantilevered toward midspan. At approximately the quarter-span, the roadway passes by the arch but is not connected to the arch. Each arch base is supported by a massive pier, and the base condition is modeled as fixed near the face of the pier. In the structural analysis model, out-of-plane displacement is restrained at the crown of the arch and at the tip of each of the cantilevered sections of the roadway at midspan. Horizontal displacement is restrained, both in-plane and out-of-plane, at the node at each end of the roadway. The roadway width from curb-to-curb is 27 ft, so two traffic lanes were used for the bridge rating. By a simple transverse analysis, it was determined that each arch supports the equivalent of 1.16 standard trucks, or traffic lanes.

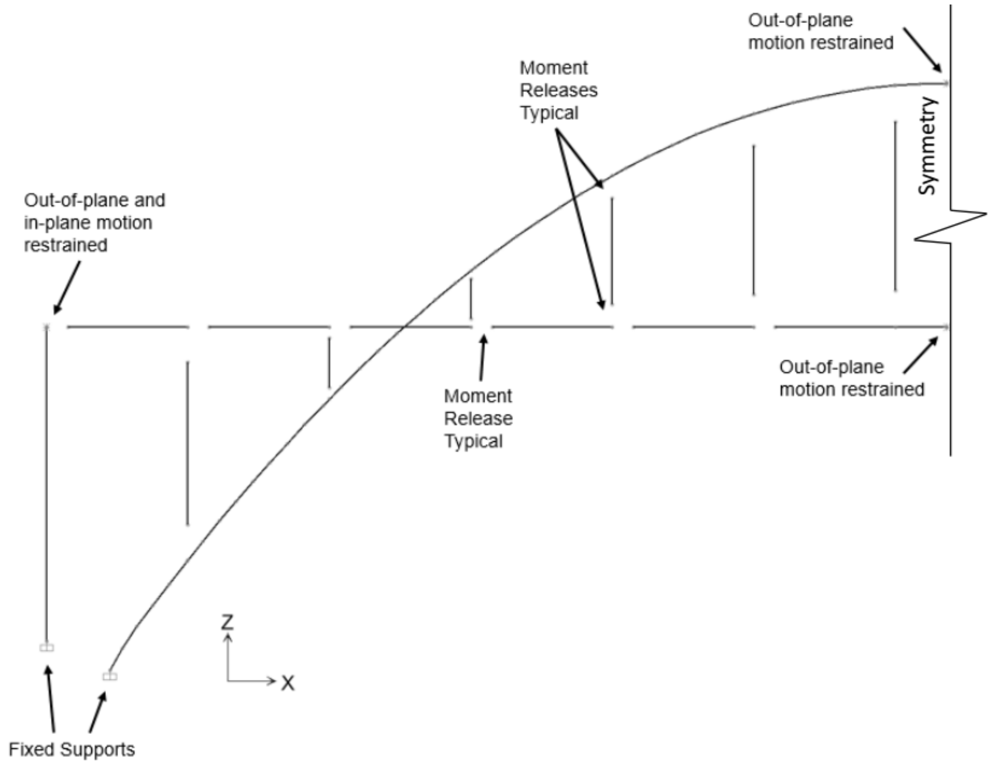

Fig. 2. Boundary conditions and restrains for half Span V (SAP2000 v. 19)

3. Approaches used to account for creep and cracking in evaluation of RC arches

Design codes provide different approaches to account for creep and cracking in evaluation of concrete structures. One simple method is to reduce flexural rigidity of the element by multiplying the gross moment of inertia of the cross section (I_g) by reduction factor. Arches as members being consistently compressed can be considered as columns. Reduction factors recommended by different design codes are presented in Table 1.

Table 1. Effective moment of inertia for modeling concrete structures (5), (6)

Element	ACI 318-11, ACI 318-14	EuroCode	AASHTO STANDARD SPEC 2002	AASHTO LRFD 2012
Concrete Columns	$0.70I_g$	$0.50I_g$	$0.85I_g$	$0.75I_g$

Another approach for long-term loading is to reduce the value of the short-term modulus of elasticity given by Equation 1 by dividing by 1 plus the ultimate creep coefficient as shown in Equation 2 (2).

$$E_c = 57{,}000\sqrt{f'_c} \tag{1}$$

$$E = \frac{E_c}{1+v_u} \tag{2}$$

where:

f'_c – compressive strength of the concrete (3000 psi) (3),
E_c – modulus of elasticity for concrete,
v_u – the ultimate creep coefficient.

AASHTO (2) provides equations for *EI* that include a reduction for cracking as well as a reduction for creep by using β_d (absolute value of the ratio of the maximum factored dead load bending moment to the maximum factored total load bending moment). Two equations for *EI* are given in AASHTO (2) Section 8.16.5.2 as follows.

$$EI = \frac{\frac{E_c I_g}{5} + E_s I_s}{1+\beta_d} \tag{3}$$

$$EI = \frac{\frac{E_c I_g}{2.5}}{1+\beta_d} \tag{4}$$

where:

β_d – absolute value of the ratio of the maximum factored dead load moment to the maximum factored total load moment,
E_c – modulus of elasticity for concrete,
E_s – modulus of elasticity for steel,
I_g – moment of inertia of the gross concrete cross section,
I_s – moment of inertia of the reinforcement about the centroidal axis of the gross concrete cross section.

AASHTO (2) allows the use of either Equation 3 or 4. These equations result in values of the flexural rigidity, *EI*, that are significantly reduced from the value calculated by simply using E_cI_g. The modifications to E_cI_g made in the numerator of these equations account for cracking along the length of the member. Dividing by the factor ($1+\beta_d$) accounts for the destabilizing effect of long-term transverse deflection of a compression member due to creep.

4. Description of the conducted analyses

Span V was chosen for these analyses, because the slenderness effects are the most significant for this span. Two kinds of analyses were conducted.

First, with constant value of E (modulus of elasticity for the concrete) and different reductions for *I* (moment of inertia). A range of values from $I = 0.15\ I_g$ to $I = 0.85\ I_g$ was investigated.

Second, analyses were conducted with a constant, reduced value of I (I = 0.85 I_g) (2) and different values of E calculated using Equation 2 for assumed values of v_u from v_u = 1.0 to v_u = 4.5. ACI 209R-92 (5) suggests that the common range of values of v_u is between 1.30 and 4.15. For the considered arch, v_u = 1.06. The low value of the ultimate creep coefficient results from adjustments from standard conditions for an average annual ambient relative humidity of (70% vs 40%), loading age (28 days) and volume-to-surface area ratio (7).

For both kinds of analyses, three critical cross sections (A02, A14 and A40) with corresponding, governing load cases were considered (Fig. 3).

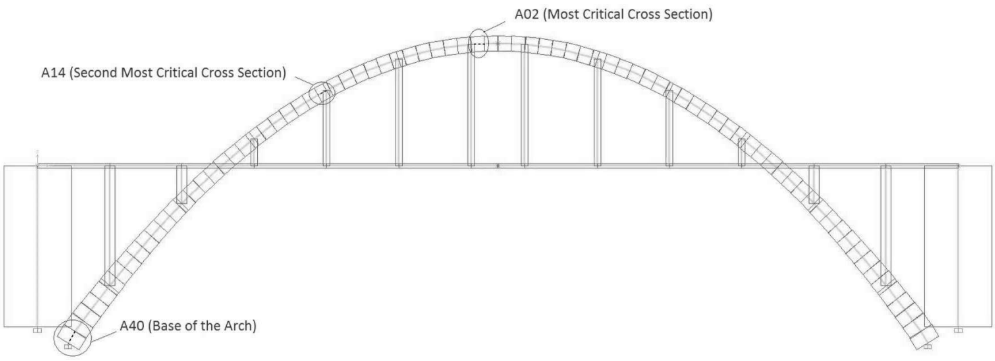

Fig. 3. General view of the Span V with locations of cross sections used for comparisons

5. Results and comparisons

Elastic second-order analysis results are compared with the results from first order analysis. The ratio between second and first order analysis result, δ, illustrates the magnification resulting from slenderness. A summary of the findings is presented in Table 2 and Table 3 and in Figures 4 through 6. In these tables and figures δ_P and δ_M mean the ratio between second and first order analysis effects for axial force and bending moment, respectively.

Table 2. Summary of results for analysis with constant E and different values of I.

Cross Section Parameter			Arch Cross Section					
			A02		A14		A40	
$Ec = E$	I	EI/E_cI_g	δ_P	δ_M	δ_P	δ_M	δ_P	δ_M
3122	0.15	0.155	1.01	1.19	1.03	1.15	1.01	1.12
3122	0.2	0.200	1.01	1.13	1.02	1.11	1.01	1.09
3122	0.3	0.300	1.01	1.08	1.01	1.07	1.01	1.05
3122	0.4	0.400	1.01	1.05	1.01	1.05	1.01	1.04
3122	0.5	0.500	1.00	1.04	1.01	1.03	1.00	1.03
3122	0.6	0.600	1.00	1.03	1.01	1.03	1.00	1.02
3122	0.7	0.700	1.00	1.03	1.00	1.02	1.00	1.02
3122	0.75	0.750	1.00	1.03	1.00	1.02	1.00	1.02
3122	0.85	0.850	1.00	1.03	1.00	1.02	1.00	1.02

Both types of analyses defined in Tables 2 and 3 result in variation of the EI, but for analyses included in Table 3, the axial rigidity of the arch (AE) is also varied. Plots of δ_M in Figures 4 through 6 show that including the reduction in axial rigidity does increase the magnification of bending moments, but not by a large amount.

Tables 2 and 3 show that the magnification of axial force in the arch is small. This is similar to the approach taken by the moment magnifier procedures in some design codes where the axial force from a first order is used along with a magnified bending moment to check a member capacity.

Table 3. Summary of results for analysis with constant $I = 0.85\ I_g$ and different values of E, (E_c = 3122 *ksi*)

Cross Section Parameter			Arch Cross Section					
			A02		A14		A40	
v_u	E	EI/E_cI_g	δ_P	δ_M	δ_P	δ_M	δ_P	δ_M
1.0	1561	0.425	1.00	1.06	1.01	1.06	1.00	1.04
1.06	1516	0.413	1.00	1.06	1.01	1.06	1.00	1.05
1.5	1249	0.340	1.00	1.08	1.01	1.07	1.01	1.06
2.0	1041	0.283	1.01	1.10	1.01	1.09	1.01	1.07
2.5	892	0.243	1.01	1.12	1.02	1.10	1.01	1.08
3.0	781	0.213	1.01	1.14	1.02	1.12	1.01	1.10
3.5	694	0.189	1.01	1.16	1.02	1.14	1.01	1.11
4.0	624	0.170	1.01	1.19	1.03	1.16	1.01	1.12
4.5	568	0.155	1.01	1.22	1.03	1.18	1.01	1.14

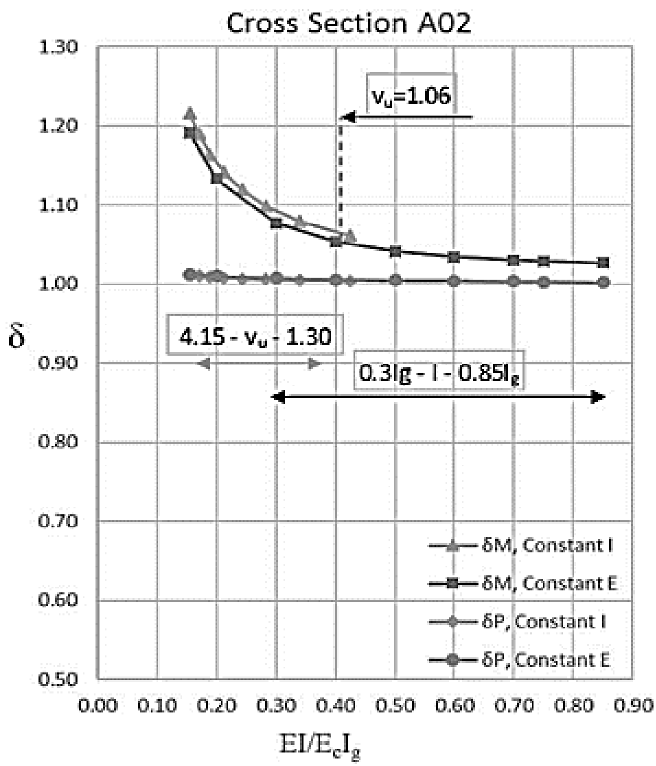

Fig. 4. Ratio of second-order to first-order results at cross section A02

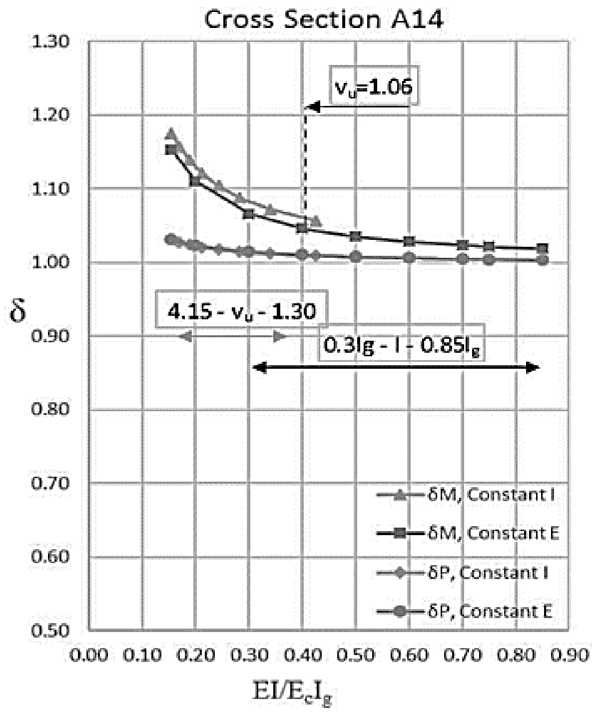

Fig. 5. Ratio of second-order to first-order results at cross section A14

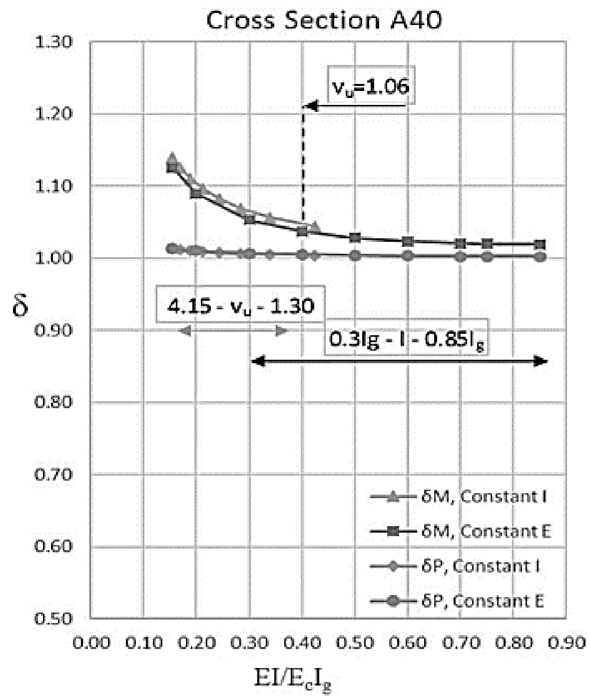

Fig. 6. Ratio of second-order to first-order results at cross section A40

The values of moment magnifier are 1.05 or smaller for (EI/E_cI_g) values of approximately 0.4 or larger. ACI 318 (9) allows designers to neglect slenderness effects in braced frame columns where the magnification is expected to be less than 5%. So, for the arch considered here, slenderness effects are not significant for (EI/E_cI_g) values of approximately 0.4 or larger. As the value of (EI/E_cI_g) decreases the amount of moment magnification increases to as much as 22% for the range of values considered here. The value of (EI/E_cI_g) decreases as the ultimate creep coefficient v_u increases. For the arch considered here, v_u is relatively small and the moment magnification is also small. But, Figures 4 through 6 illustrate that the slenderness effects become significant for concretes prone to significant creep deformations.

6. Conclusions

A summary of the methods commonly used for including creep and cracking in evaluation of reinforced concrete arch bridge ribs was presented. Two kinds of structural analyses were conducted for the considered concrete arch. In first, there was implemented the wide range of reduction factors for gross moment of inertia, in second there was implemented the wide range of reduction factors for modulus of elasticity of the concrete (using v_u – the ultimate creep coefficient). Both approaches were checked from sensitivity point of view and compared with each other. The reduction of axial rigidity through AE increases the magnification of bending moments, but not by a large amount. The magnification of axial force was small for all cases. The moment magnification is also not significant (less than 5%) for values of $EI/E_cI_g = 0.4$ or larger. For the arch studied here, the moment magnification was as much as 22% for large values of ultimate creep coefficient. This illustrates that the slenderness effects can be significant for concretes prone to large creep deformations.

References

1. The Manual for Bridge Evaluation, 2nd ed. AASHTO, Washington, D.C., 2011
2. Standard Specifications for Highway Bridges, 17th ed. AASHTO, Washington, D.C., 2002.
3. Le, T.H. and J.M. Stallings: Load Rating of the Bibb Graves Concrete Arch Bridge. Final Report 930–858. Auburn University Highway Research Center, Auburn University, Auburn, AL, 2014.
4. Le, T.H. and J.M. Stallings: Slenderness Effects in Reinforced Concrete Arch Bridges. Transportation Research Board 94th Annual Meeting, paper numbers: 15-2352, 2015.
5. Wong J-M, Sommer A., Briggs K., Ergin C.: Effective, Stiffness for Modeling Reinforced Concrete Structures, Structure Magazine, pp. 18–20. January 2017.
6. AASHTO LRFD Bridge Design Specifications, 6th ed. AASHTO, Washington, D.C., 2012.
7. Prediction of Creep, Shrinkage and Temperature Effects in Concrete Structures. ACI209R-92. American Concrete Institute, Farmington Hills, MI, 1992.
8. Building Code Requirements for Structural Concrete (ACI 318-14) and Commentary (ACI 318R-14), Farmington Hills, MI, 2014.
9. CSI Analysis Reference Manual, SAP2000 v.19, Computers and Structures, Inc., Berkeley, CA, 2015.